The Journal of Experimental Biology 205, 1339–1353 (2002)
Printed in Great Britain © The Company of Biologists Limited 2002
JEB4011



# Torque patterns of the limbs of small therian mammals during locomotion on flat ground

Hartmut Witte*, Jutta Biltzinger, Rémi Hackert, Nadja Schilling, Manuela Schmidt, Christian Reich and Martin S. Fischer

*Institut für Spezielle Zoologie und Evolutionsbiologie, Friedrich-Schiller-Universität Jena, Erbertstraße 1, D-07743 Jena, Germany*

*e-mail: hartmut.f.witte@gmx.de

*Accepted 12 February 2002*

## Summary

**In three species of small therian mammals (Scandentia: *Tupaia glis*, Rodentia: *Galea musteloides* and Lagomorpha: *Ochotona rufescens*) the net joint forces and torques acting during stance phase in the four kinematically relevant joints of the forelimbs (scapular pivot, shoulder joint, elbow joint, wrist joint) and the hindlimbs (hip joint, knee joint, ankle joint, intratarsal joint) were determined by inverse dynamic analysis.**

**Kinematics were measured by cineradiography (150 frames $s^{-1}$). Synchronously ground reaction forces were acquired by forceplates. Morphometry of the extremities was performed by a scanning method using structured illumination.**

**The vector sum of ground reaction forces and weight accounts for most of the joint force vector. Inertial effects can be neglected since errors of net joint forces amount at most to 10 %. The general time course of joint torques is comparable for all species in all joints of the forelimb and in the ankle joint. Torques in the intratarsal joints differ between tailed and tail-less species. The torque patterns in the knee and hip joint are unique to each species.**

**For the first time torque patterns are described completely for the forelimb including the scapula as the dominant propulsive segment. The results are compared with the few torque data available for various joints of cats (*Felis catus*), dogs (*Canis lupus* f. *familiaris*), goats (*Capra* sp.) and horses (*Equus przewalskii* f. caballus).**

Movies available on-line.

Key words: Torque pattern, limb, small therian mammal, *Tupaia glis*, *Galea musteloides*, *Ochotona rufescens*, locomotion, stance phase, inverse dynamics.

## Introduction

Kinematic studies of 14 species of small mammals revealed a high interspecific uniformity of locomotion patterns (Fischer, 1994, 1998, 1999; Fischer and Witte, 1998; Fischer and Lehmann, 1998; Schilling and Fischer, 1999; Schmidt and Fischer, 2000; Fisher et al., 2002). We conducted experiments to determine the mechanical needs and boundary conditions that urge the strong convergence (or persistence?) of limb geometry and kinematic functions. In addition to studies on kinematics, energetics and control of locomotion (e.g. Alexander and Goldspink, 1977; Cavagna et al., 1977; Ganor and Golani, 1980; Alexander, 1988; Kuznetsov, 1995; Full and Koditschek, 1999), empirical knowledge is required about the dynamic function and the structural properties of the small mammalian locomotor apparatus. Here, we raise the question of whether the uniform kinematics are reflected by equivalent uniform dynamics.

To answer this question, we need synchronous measurements of the net joint forces and the net joint torques that occur in the eight kinematically relevant joints of mammalian forelimbs and hindlimbs (Fischer, 1994, 1998, 1999) (Fig. 1). A complete data set such as this is not yet available, because most studies have focussed on the three proximal joints of the hindlimb of several larger animals (Pandy et al., 1988; Dogan et al., 1991; Fowler et al., 1993; Perell et al., 1993; Colborne et al., 1997; Clayton et al., 1998).

The kinematics of the extremities are similar in all the small mammalian species studied by our group. Two further elements of the postcranial locomotor apparatus may also strongly influence locomotion: the trunk and the tail. For the purposes of this study we choose three species that exhibit show maximal differences in the proportions of the trunk and the existence of a tail: *Ochotona rufescens* (the pika), *Galea musteloides* (the cui), and *Tupaia glis* (the tree shrew). The pika has a short trunk and no tail. The cui is tail-less like the pika, but has a long trunk. The tree shrew has a body shape comparable to that of the pika, but has a tail. According to Fisher et al. (2002), the pika is typical of tail-less species kinematics, the tailed tree shrew shows behaviour typical of tailed species, while the tail-less cui exhibits elements of tail-less kinematics (e.g. in the moment of the pelvis).

Direct measurements of internal body forces are only feasible for single elements of the locomotor apparatus. Forces within a volume of more than 5 cm×5 cm×5 cm may be determined non-invasively using magnetic resonance techniques, but to date has only been performed under static loading conditions (Witte et al., 1997). Using more invasive approaches, tendon forces (Biewener et al., 1988, 1995; Fowler et al., 1993; Jansen et al., 1993; Gregor and Abelew, 1994; Malaviya et al., 1998) and joint forces (Graichen and Bergmann, 1988, 1991; Kotzar et al., 1991; Bergmann et al., 1993; Brand et al., 1994) have been recorded using implanted sensors. No technique has been reported for direct measurement of joint torques and no study has attempted to measure forces simultaneously in forelimbs and hindlimbs.

The internal forces of a limb can be estimated from the ground reaction forces (GRF), weight and inertial forces provoked by movements. The method we have used is the 'inverse dynamics approach' IDA (Manter, 1938; Bresler and Frankel, 1950, here applied in the Newton–Eulerian version, as described by Hoy and Zernicke, 1985). This method quantifies the dynamic effects of the GRF, reflecting the dynamics of the whole body (i.e. in relation to those of the inertia and weight of the segments distally of the joint under observation). Although inertial and gravitational effects can be separated by controlled disturbances of motions, this study is on physiological motion patterns only (cf. Chang et al., 2000). The observations were limited to the stance phase of regular, cyclic locomotion on flat ground. Animals were subjected to a range of speed and gait patterns achieved under minimised restraint and the animals' autonomy. In contrast to earlier studies, the scapula (i.e. the first proximal segment) was included in the analyses, since the kinematic data clearly indicate that the scapula and its musculature are the main propulsive elements of the forelimb in therian mammals (Fischer, 1999).

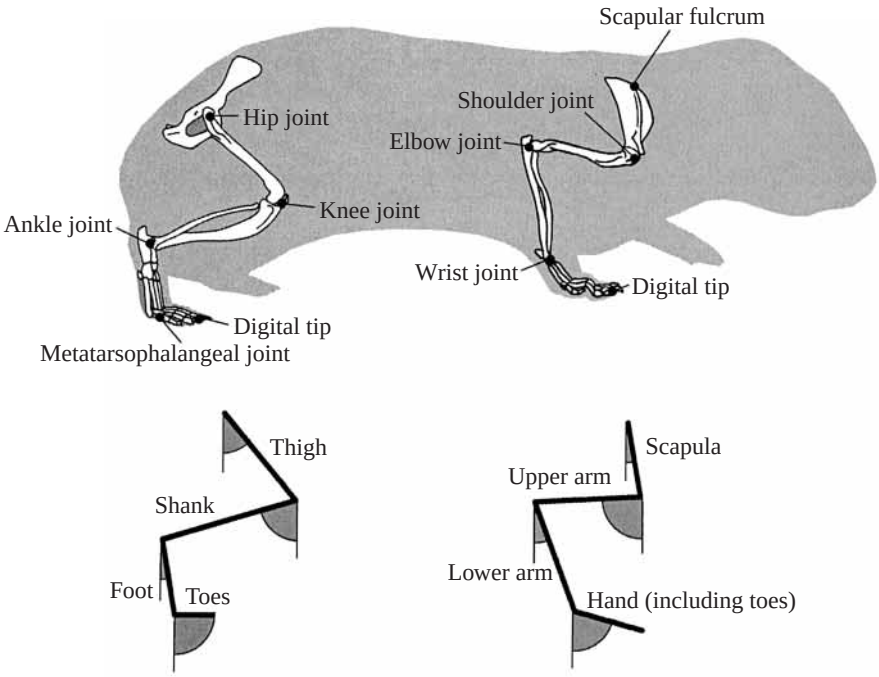


Fig. 1. The four long segments of a mammalian extremity. Forelimb: scapula, upper arm, lower arm and hand, linked to the proximal segment by scapular fulcrum, shoulder joint, elbow joint and wrist joint. Hindlimb: thigh, shank, foot and toes, linked to the proximal segment by hip joint, knee joint, ankle joint and metatarsophalangeal (intratarsal) joint.

## Materials and methods

### *Animals*

All animals were kept according to the German animal welfare regulations. The experiments were registered by the Committee for Animal Research of the Freistaat Thüringen, Germany.

Kinematic and force data were collected to confirm the high interspecific uniformity of kinematics observed in earlier studies. We then focussed on one individual of each species for the inverse dynamics analysis (IDA).

The lagomorph *Ochotona rufescens* Gray 1842 (the pika) lives in the central Asian steppes. We used male animals ranging in body weight (BW) from 190 g to 260 g, and in crown-rump length (CRL) from 19 cm to 22 cm. For morphometric measurements, we used an animal of 220 g BW with a CRL of 20 cm. Kinematic reference data were taken from four animals running on flat ground, GRF from six individuals. IDA was carried out on an animal of 210 g BW (CRL 20 cm). An extensive kinematic study has already been published (Fischer and Lehmann, 1998).

The rodent *Galea musteloides* Meyen 1832 (the cui) is an inhabitant of the Andesian pampa. In our breeding colony, adult animals show a BW of 300–400 g and an average CRL of 22 cm. Kinematic reference data were obtained from four individuals running on a treadmill and five animals moving on flat ground. In addition, reference GRF were recorded could be taken from six individuals. Morphometry was performed on a female individual of 350 g BW and 22 cm CRL. Inverse dynamics were illustrated for one female individual of 350 g BW and 21 cm CRL. Kinematic data have already been published (Fischer, 1999).

*Tupaia glis* Diard 1820 (Scandentia; the common tree shrew) lives in rainforests in Southeast Asia. The animals under study had a BW of 150–210 g, CRL was 14–23 cm and tail length (TL) 13–20 cm. Kinematic reference data were recorded from two individuals running on a treadmill and flat ground. Morphometric data were taken from an animal of 160 g BW, 15 cm CRL and 14 cm TL. IDA was performed on a female animal (BW 150 g, CRL 14 cm, TL 13 cm). Kinematic data can be found in Schilling and Fischer (1999).

### *Dynamics analysis*

IDA is based on rigid body dynamics and requires three kinds of input data: (1) morphometric data like length and mass properties (masses, $m_I$, and mass moments of inertia, $I_i$) for all of the system elements *i*, (2) kinematics and (3) externally applied forces and torques (which in terms of mechanics are called 'generalised forces', described by vectors with six elements) like ground reaction forces (GRF) or ground reaction torques (GRT).

### *Morphometric analyses*

Morphometric analyses were performed on animals sacrificed for that particular purpose. They were similar to sacrificed animals (i.e., with similar BW and CRL). Morphometric data were scaled geometrically to extrapolate the animals of different body size (cf. Pedley, 1977; Calder, 1984; on the sensitivity of IDA to body segment parameter variations cf. Andrews and Mish, 1996; Nagano et al., 2000). To derive volume models of the animals' limbs, several techniques of maximum spatial resolution were tested (CT, 80 μm; MRI, 300 μm; laser surface scans, 200 μm). The acquisition of surface scans emerged as the most practical procedure and was therefore applied to all species. The animals were skinned to determine the thickness of the coat at the limbs. The exarticulated limbs were moulded and scanned using a customised structured light illumination method provided by the Fachhochschule Jena. To the volume models of the limbs' segments, we added the thickness of the skin (i.e. computationally 'recoating' the animal). We then calculated the masses, mass moments of inertia and the principal axes, assuming an average density of 1.1 g cm$^{-3}$. This average was obtained from densitometry on fresh unfrozen specimen (cf. Winter, 1990; Fung, 1993), and was confirmed by our own density measurements using fluid displacement methods (Table 1).

### *Kinematics*

Kinematics in the current analysis were analysed as before (Fisher et al., 2000) using uniplanar cineradiography. The restriction of kinematic measurements to a single plane (2-D analysis) in contrast to the conditions in human beings (Eng and Winter, 1995; Glitsch and Baumann, 1997), is acceptable as long as the animals run in a plane perpendicular to the X-ray beam and move their limbs parasagittally. To ensure that these conditions were being met, the animals in the experiments were restrained within a small (12 cm width) Plexiglass walkway with a length of 2 m or 3 m, depending on the velocity we wanted to provoke.

Cineradiographies were recorded at 150 Hz. The images were generated by a Philipps® system 9807 501 800 01 at the Institut für den Wissenschaftlichen Film (Göttingen). Data documentation used a Mikromak® Camsys® high-speed-video system with three cameras recording images synchronously. One camera filmed the X-ray sequence from the image amplifier, while the other two recorded the moving animal in normal light. Kinematic data analysis was performed interactively on grabbed video frames with a custom-made software (Unimark by R. Voss). Distortions of the X-ray maps were corrected by reference to a grid of steel balls (diameter 1.00±0.01 mm, with a mesh width of 10.0±0.05 mm), filmed before and after each experimental session. To minimize systematic errors during the digitisation process, all frames were analysed by the same people who had created an earlier database on small therians' locomotion (Fisher et al., 2000) and, therefore, had the greatest experience (cf. the remarks of Plagenhoeft, 1979 on the influence of the investigator's morphological knowledge on the results of motion analyses).

To control for operator errors in the digitisation procedure, we carried out repetitive analysis of 25 frames from randomly chosen sequences five times each. We discovered that the extent of the error was dependent on the size of the animal.

Table 1. *Properties of the segments of the extremities in the three species under study*

| | Mass (g) | *I* (g cm$^2$) | *L* (cm) | CoM I (%) | CoM II (%) |
|---|---|---|---|---|---|
| *Galea musteloides* | | | | | |
| Hand | 0.55 | 0.13 | 1.48 | 50 | 0 |
| Lower arm | 1.32 | 1.01 | 3.44 | 45 | –2 |
| Upper arm | 7.06 | 8.58 | 3.29 | 25 | –1 |
| Scapula | 7 | 8 | 3 | 50 | 0 |
| Toes | 0.14 | 0.02 | 0.96 | 50 | 0 |
| Foot | 0.57 | 0.57 | 1.92 | 42 | –17 |
| Shank | 3.94 | 2.89 | 4.35 | 45 | –1 |
| Thigh | 15.6 | 30.4 | 3.47 | 43 | 11 |
| *Ochotona rufescens* | | | | | |
| Hand | 0.39 | 0.34 | 1.89 | 50 | 0 |
| Lower arm | 1.14 | 0.86 | 2.37 | 31 | 0 |
| Upper arm | 3.01 | 5.46 | 2.71 | 54 | 15 |
| Scapula | 1.54 | 2.65 | 2.62 | 42 | 9 |
| Toes | 0.14 | 0.07 | 0.89 | 55 | 0 |
| Foot | 0.59 | 0.21 | 1.79 | 60 | 2 |
| Shank | 2.05 | 4.00 | 3.87 | 48 | 2 |
| Thigh | 8.13 | 12.2 | 2.75 | 36 | 2 |
| *Tupaia glis* | | | | | |
| Hand | 0.65 | 0.17 | 1.61 | 50 | 0 |
| Lower arm | 1.24 | 0.72 | 3.05 | 46 | –14 |
| Upper arm | 4.51 | 3.65 | 2.93 | 40 | 2 |
| Scapula | 2.52 | 1.73 | 2.71 | 52 | 0 |
| Toes | 0.26 | 0.06 | 1.11 | 50 | 0 |
| Foot | 1.06 | 0.91 | 2.21 | 54 | 4 |
| Shank | 4.50 | 7.72 | 4.55 | 44 | –3 |
| Thigh | 11.1 | 24.7 | 3.46 | 37 | –15 |

*G. musteloides*, body mass=350 g, crown–rump length (CRL)= 22 cm; *O. rufescens*, body mass=220 g, CRL=20 cm; *T. glis*, body mass=160 g, CRL=15 cm, tail length=14 cm.

*m*, mass; *I*, mass moment of inertia around the proximal joint; and *L*, length as the distance along the axis from the proximal to the distal joint, are all given as absolute values.

The position of the center of mass (CoM) is relative to the axis of the segment: CoM I, proximo–distal; CoM II perpendicular to the axis (positive values indicate a caudally oriented deviation).

Table 2. *Characteristics of the two Kistler® force plate systems used*

| | Force plate 1 | | | Force plate 2 | | |
|---|---|---|---|---|---|---|
| Direction | Craniocaudal (*x*) | Medio-lateral (*y*) | Vertical (*z*) | Craniocaudal (*x*) | Medio-lateral (*y*) | Vertical (*z*) |
| Resonance frequency (Hz) | 2500 | 1471 | 2041 | 2500 | 1389 | 2778 |
| $t_{\frac{1}{2}}$ (ms) | <0.1 | <0.5 | <0.5 | <0.1 | <0.5 | <0.5 |
| | Chain 1 | | | Chain 2 | | |
| Base level of noise (mN) | 0.2 | 0.25 | 0.1 | <0.1 | 0.25 | <0.1 |
| Peak of noise | | | | | | |
| Frequency (Hz) | 78.2 | 78.2 | 78.2 | 78.2 | 49.2 | 78.4 |
| Amplitude (mN) | 2.5 | 2 | 2 | 2.7 | 1.3 | 1.5 |
| Second peak of noise | | | | | | |
| Frequency (Hz) | – | – | 100–103 | – | – | – |
| Amplitude (mN) | – | – | 1 | – | – | – |

The 78 Hz peak of noise is caused by the main frequency of the computer monitor of the force measuring system.
$t_{\frac{1}{2}}$, time for reduction of amplitudes to half the maximum after exciation of the force plate with a hammer.

The maximum overall error of digitisation was ±0.6 mm for coordinate values, 0.5–2.0 ° for angles describing the segment orientation in the global frame and 1°–3 ° for joint angles, according to the Gaussian theorem on error propagation. Based on control measurements of a compound pendulum, these sources of measurement errors led to an overall noise level of ±0.4 mm, 0.4 ° for segment angles and 0.6 ° for joint angles.

The trajectories of the segments' centers of mass (CoM) were calculated from the joint trajectories in combination with the morphometric results. To enable synchronisation of kinematic and force data and to reduce the noise in the twofold numerical derivation necessary for the determination of accelerations and angular accelerations, we used several techniques (smoothing, splines, fourier and polynomal fits) proposed in the literature (for their use in biomechanics, cf. especially Hatze, 1981; Challis, 1997; Koopman et al., 1995). We opted for a polynomal fit of second to sixth order. Deviations from polynomals of higher order were within the range of the $\chi^2$-estimation of the predicted error. The remainder term of higher than sixth order in all cases was lower than 0.5 % (this value giving the termination criterion).

*External forces*

External forces acting on the animals (neglecting air resistance) are GRF and GRT. GRF and GRT were measured with two specially designed Kistler® force plates. The aluminium alloy surfaces of the platforms were coated with cork of 1 mm thickness which was also glued onto the walkways, in order (a) to avoid unphysiological hard contacts (some of the species under study show an initial spike in their GRF-patterns), (b) to facilitate frictional force transfer and (c) to adapt the compliance and aspect of the force plates to that of the walkway. On sensitive areas of the force plate (120×200 mm), vertical forces up to 1 kN and horizontal forces up to 0.2 kN could be determined. The manufacturer Kistler® guarantees that for vertical forces within the range of our experiments (i.e. 1 N), the maximal linear calibration error should be less than 10 % (0.1 N). In static calibration controls we identified a maximal error of 1.3 % for forces of 0.1–1 N. In standardised dynamic control experiments, with bouncing rubber and steel balls, the force–time relationships were reproducible with a correlation coefficient of minimally 96.4 % in ten consecutive trials each. Since the resonance frequencies of the platforms are between 1.5 kHz and 2.5 kHz, depending on the measuring direction and the mode of vibration (Table 2), Nyquist's and Shannon's theorem of sampling harmonic data requires reference GRF measurements at 6.125 kHz. This sampling frequency was at the limits of our A/D-converter and could not be reached reliably in all trials. We therefore reduced the sampling frequency to 3.6 kHz during the routine measurements for IDA. The maximal noise of the two complete data acquisition chains, comprising a force platform, conductions, amplifier, analogue-digital-converter and computer, was 2.7 mN with a base level of noise of maximally 0.25 mN (Table 2). Since noise levels were dependent on the combination of devices used in each chain, the two combinations with the lowest noise were used throughout the entire experiment. On completion of the study, noise levels were experimentally determined to be unchanged.

Acquisition of kinematic data and GRF/GRT was triggered by an external manual switch and electronically synchronised. The error of synchronisation was 1.800±0.050 ms, equivalent to a timing difference of less than one-third of a video frame. Data were included in the study if single limb contact on one force plate could be identified without any doubt, and if the corresponding X-rays allowed reliable identification of joint landmarks.

The four rigid bodies that we analysed on the forelimbs are the scapula, upper arm, lower arm and hand, and on the hindlimbs, the thigh, shank, foot (metatarsus and tarsus) and toes (represented by the longest toe in contact with the ground) (Fig. 1). This analysis corresponds to the proposals of the International Society of Biomechanics (ISB). In deviation from this right handed system, all calculated joint torques

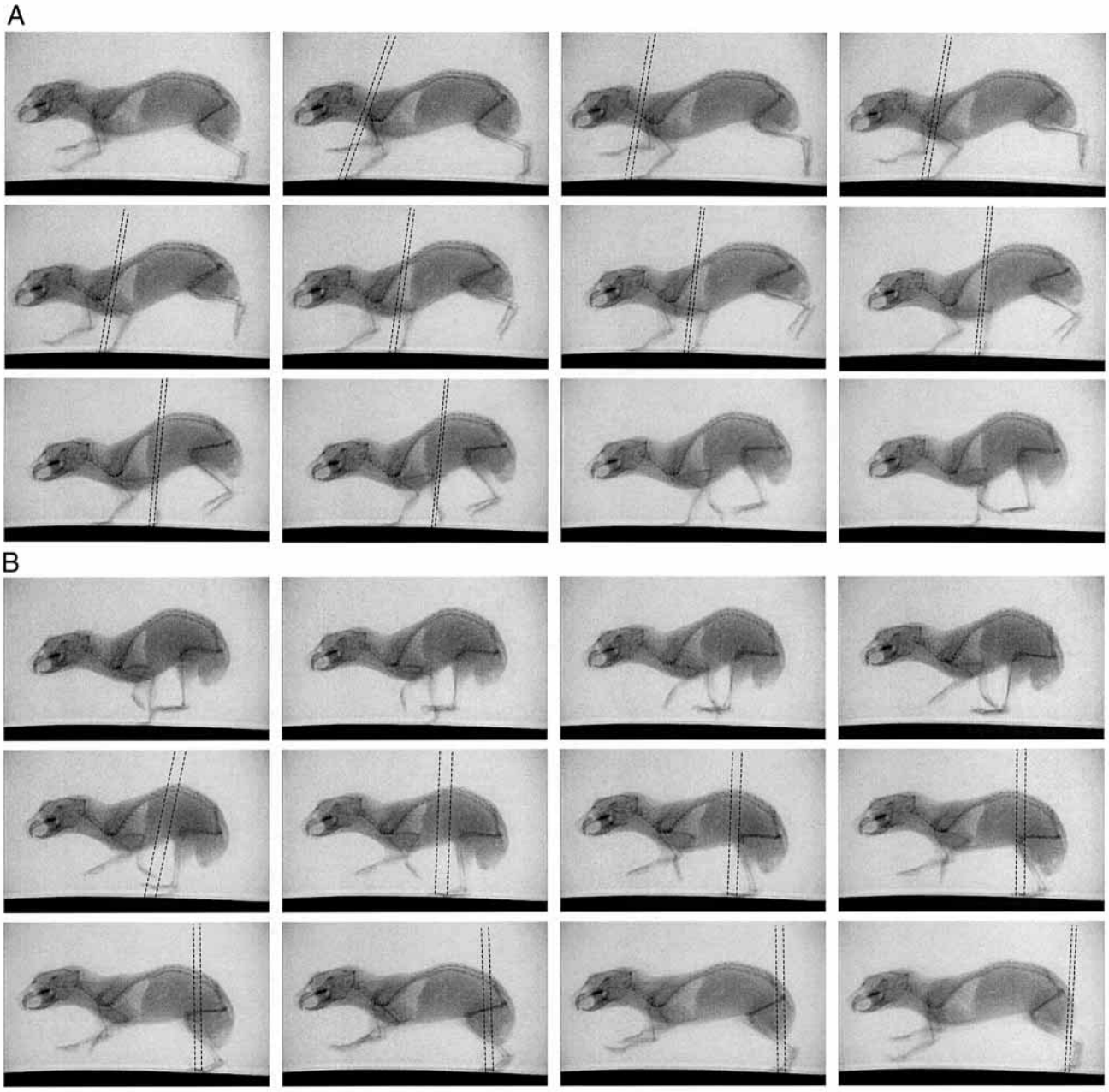


Fig. 2. Range for the possible lines of actions of ground reaction forces (GRF) in a pika (*Ochotona rufescens*) during half-bound. The Center of Pressure (CoP) may be located anywhere under the sole of the foot. The effects are illustrated for one forelimb (A) and one hindlimb (B).

were defined to be positive if the torque tended to extend the joint; i.e. to work against gravitational collapse of a standing limb. The scapular pivot in our preceding kinematic studies could reliably be located at the dorsal end of the scapular spine.

Neither the cineradiography nor the force plates resolved the center of pressure (CoP) of GRF acting on one foot with sufficient accuracy. Thus, we had to assume this application point of GRF to be constant during stance, except after lift-off of the heel. CoP was defined to be located in the centre of the sole. Fig. 2 indicates the possible error caused by this assumption for a half-bound cycle of a pika. At the end of stance, after visible lift-off of the heel, the application point of GRF was assumed to be under the toes.

The forces measured and calculated were normalised to BW. To allow quantitative interspecific comparisons of torques, the graphs are normalised in two ways:

(1) For comparison of the amplitudes of torques, the graphs are normalised to BW. Alternate approaches taking into account the effects of changing lever arms, normalise torques by $BW^{1.33}$ (geometrical scaling) or $BW^{1.375}$ (elastic scaling). This normalisation procedure did not alter substantially and of our interspecific comparisons.

(2) The BW of the animals was not always available for data

taken from literature. Therefore, to enable the comparison of all data sets, we normalised to BW by:

$$\int M(t)dt = 1\,, \tag{1}$$

or, since the time of ground contact may be normalised to be

$$t = 1\,, \tag{2}$$

this is equivalent to

$$\bar{M}(t) = 1\,, \tag{3}$$

where $t$ is ground contact time (s) and $M$ is torque (N m).

## Results

Small animals in unrestrained conditions either show exploratory movements, seemingly unsystematic walking behaviour or (mainly in escape situations) fast gaits. Continuous cyclic locomotion in small mammals is an idealised concept. Longer episodes can only be provoked by training (i.e. positive or negative feedback) or by the use of walkways. The results reported here have to be qualified as 'acquired under minimal restraint'.

Under these conditions, the species in question reproducibly showed fast gaits, with *G. musteloides* preferring symmetrical gaits, and *O. rufescens* and *T. glis* in-phase gaits. From more than 200 sequences, only 29 were processed further, after strict validation. Since the physiological time scale of small mammals is short relative to that of large animals like humans (cf. Calder, 1984), we accepted locomotion to be cyclic if at least three complete movement cycles could be recorded without any observable pause. Changes in the phase relations of the interlimb coordination patterns during these cycles were accepted, since small mammals tend to change their gait patterns continuously (cf. Heglund et al., 1974, 1982; Taylor et al., 1982; Calder, 1984).

In contrast to our assumptions, the CoP may be localised anywhere under the sole of the foot (Fig. 2). Fig. 3 shows the result of our sensitivity analysis in *O. rufescens* to shifting the

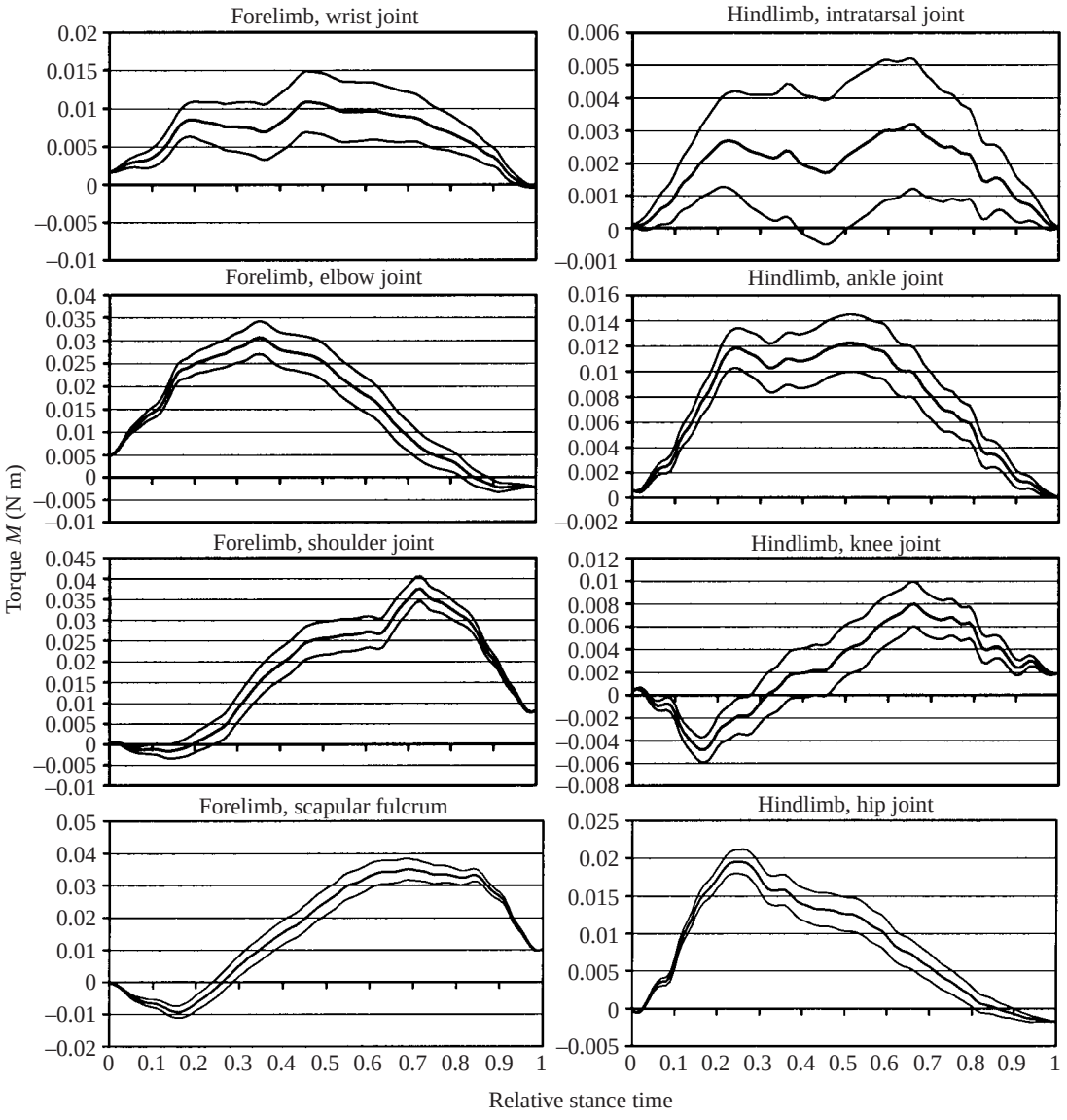


Fig. 3. Sensitivity analysis: effect of the possible mislocation of the center of pressure CoP in *Ochotona rufescens* illustrated in Fig. 2 on the torques in the joints shown in Fig. 1. Graphs are given for a half-bounding pika for assumed locations of the CoP under tip of toe and heel (thin lines) and midsole (thick lines).

line of action of GRF under the foot sole on the joint torques. The error provoked is maximal in the pika. The amplitude of the joint torques may be in error by ±100 % in the distal joints. This error gradually reduces to ±15 % in the proximal joints. The maximal errors may occur during midstance. The time course of the joint torques is not substantially affected by this error, wrong signs (directions) in the torques may only be provoked in the intratarsal joints of the pika.

The GRF measurements used for IDA (Fig. 4) are in agreement with the results of some 300 measurements not used for IDA. During stance, pika and cui carry up to 160 % of BW on the forelimb, while the hindlimbs are loaded by up to 60 % (pika) and 90 % (cui). The tree shrew shows a maximal GRF of 90 % BW on both the forelimbs as on the hindlimbs. The GRT transmitted through the point-like contacts of the feet to the ground did not differ significantly from the basic noise. For IDA calculations we assumed them to be zero.

No systematic interdependencies were found between the shape of the single limbs' GRF (Fig. 4A,B) or its integrated value (indicating the momentum inferred), and the overall motion state of the body. From several additional GRF-measurements, including simultaneous motion analysis of the animals' trunk, we know that a net braking effect of one or two legs in combination with a net acceleration of other limbs is common. The roughly half-sine shape of the vertical GRF indicates that elastic bounce (cf. Alexander, 1988; Full et al., 1991) may have relevance even in small mammals.

In agreement with the results of kinematic studies relating proximal segments to the spatial gain of the

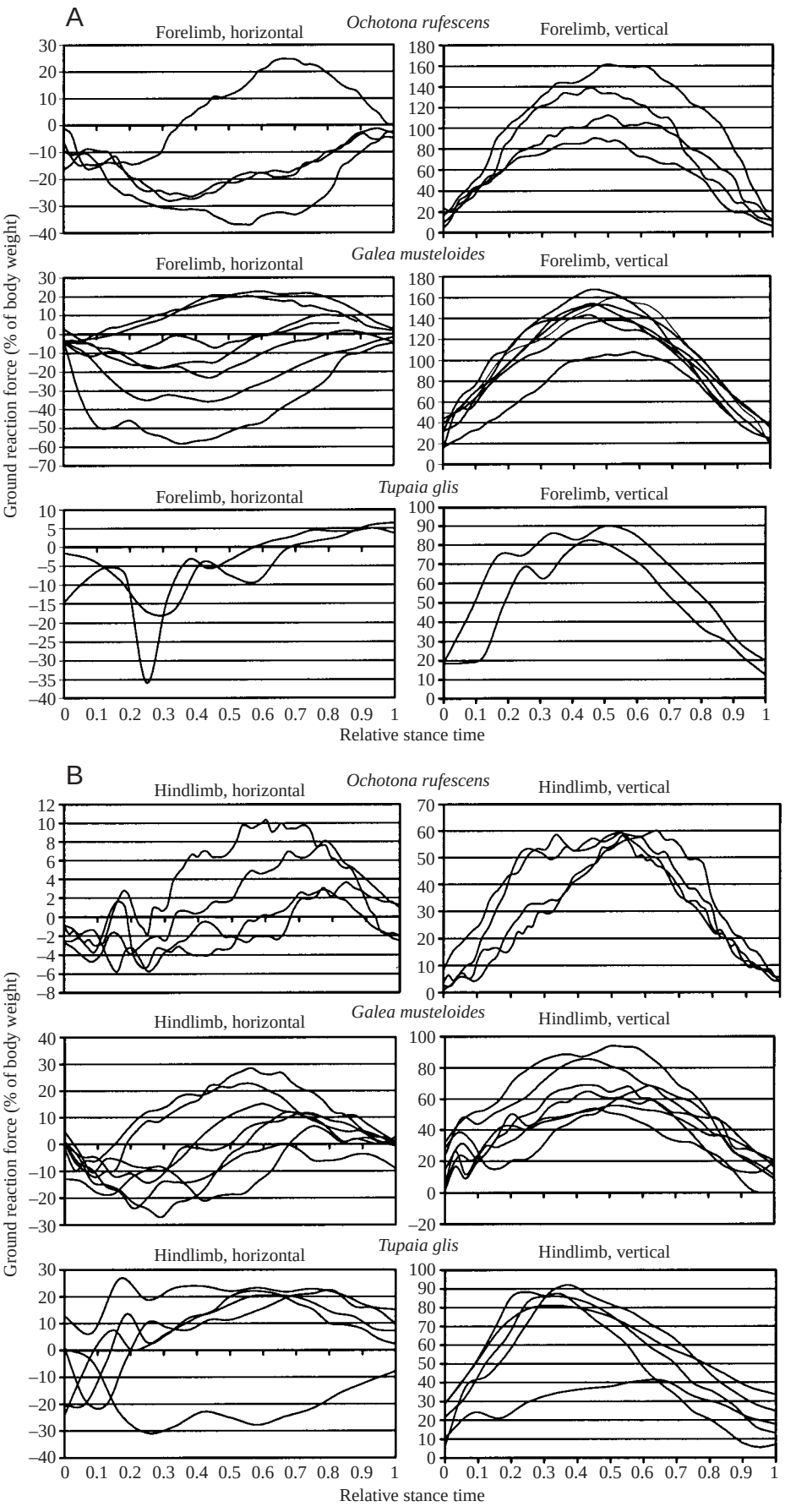


Fig. 4. Ground reaction forces (GRF) in *Galea musteloides*, *Ochotona rufescens* and *Tupaia glis*, measured in the 29 trials used for inverse dynamic analysis. Left, horizontal forces, positive values indicate forces acting in the direction of propulsion; right, vertical forces. (A) Forelimbs; (B) hindlimbs.

extremities' movement cycles (Fischer and Lehmann, 1998; Fisher et al., 2002), the interdependency between the integrated value of the of horizontal GRF and joint torques is higher the more proximally the joint is located. The most extreme case occurs in the scapular pivot, where the torque pattern may be 'shifted' between the upper and the lower limit of torques even within the same cycle. These patterns are more reproducible in the forelimbs than in the hindlimbs, in part due to the fact that we observe the occurrence of 'initial spikes' in the GRF-patterns of mostly the hindlimbs. This directly affects the shape of the torque patterns and increases their variability. For the distal joints, we were unable to identify any systematic influence of the propulsive horizontal forces on the amplitude or shape of the joint torques.

The joint force vectors in the small mammals more or less are ruled by GRF (Fig. 5). Inertial effects and weight are negligible except for the proximal segment (scapula, femur) (cf. the same effect in humans described by Krabbe et al., 1997). The resultant joint forces exceed GRF by maximally 10 % (16 % BW).

Amplitudes of the torque patterns are normally distributed (Fig. 6; Kolmogorov–Smirnov, $P<0.01$).

The main component of joint torques is provided by GRF (Fig. 7). Its amplitude may be higher or lower than the net joint torque. In the distal joints, inertia and weight effects may account for up to 60 % of the GRF component, reducing the net joint torques. In the proximal joints, this share is maximally 50 %, increasing net joint torques.

The torque patterns on the forelimbs are similar, independent of species or gait pattern (Fig. 8). In the wrist joint, torque increases and decreases in a harmonic monophasic and symmetrical manner. In the elbow joint, the torque peaks at about one-third of stance, with low flexing torques in late stance. The time course of the shoulder joint torque is more or less symmetrical around a peak two-thirds into the stance. This time course resembles the torque in the scapular pivot. The main difference arises from a flexing component, causing the shoulder joint to exhibit a biphasic time course.

Torque in the hindlimb shows a greater interspecific variability. In the intratarsal joint, the monophasic torque peaks in *T. glis* (the tailed species) in the early third of stance, and in *O. rufescens* and *G. musteloides* (the tail-less species) in the late third of stance. This pattern for *T. glis* remains the same in the ankle joint, while in *O. rufescens* and *G. musteloides*, the maximum occurs during midstance. In the knee joint, the monophasic torque graphs of *G. musteloides* and *T. glis* peak at midstance, while *O. rufescens* shows a biphasic behaviour: a small maximum of flexing torques in early stance is followed by a more or less half-sine shaped extending torque of twice that amplitude in the two last thirds of stance. In the hip joint, large interspecific differences occur.

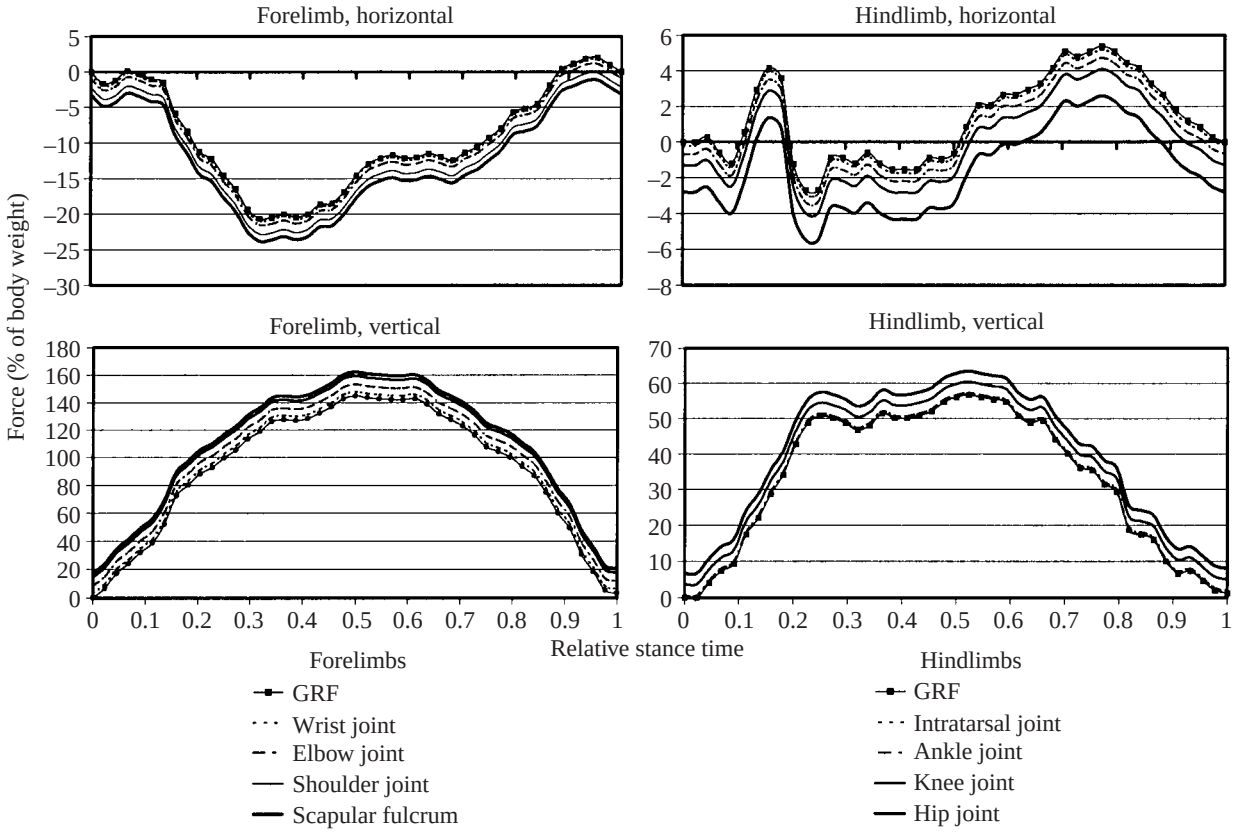


Fig. 5. Components of net joint forces in a half-bounding pika (*Ochotona rufescens*). Left, forelimbs; right, hindlimbs; top, horizontal; bottom, vertical.

*O. rufescens* and *G. musteloides* provide a monophasic torque graph: *O. rufescens* with a maximum in the first third of stance; *G. musteloides* in the last third of stance. In *Tupaia*, the graph is asymmetrical: starting with flexing torques in early stance, a burst of extending torques at 20 % of stance is followed by a wider maximum of flexing torques in the second half of stance.

## Discussion

The uniform kinematics of small mammals observed in earlier studies reflect equivalently uniform dynamics. Remarkable interspecific differences are found in the torques acting on the proximal joints of the hindlimbs. This observation indicates that the pelvis is used as an additional 'segment' in synchronous gaits (Fisher et al., 2002), which cannot be registered by IDA of the limbs, and could not be separated from species-specific effects or the interaction with a tail.

The three small mammals studied here as well as the other 11 mammalian species we studied before do not show the kind of cyclic locomotion we normally associate with endurance locomotion in larger mammals like humans and small domestic animals. It simply makes no sense for small movements to move over long distances during longer time periods in an open environment using continuous cyclic movements. In contrast to earlier more general statements

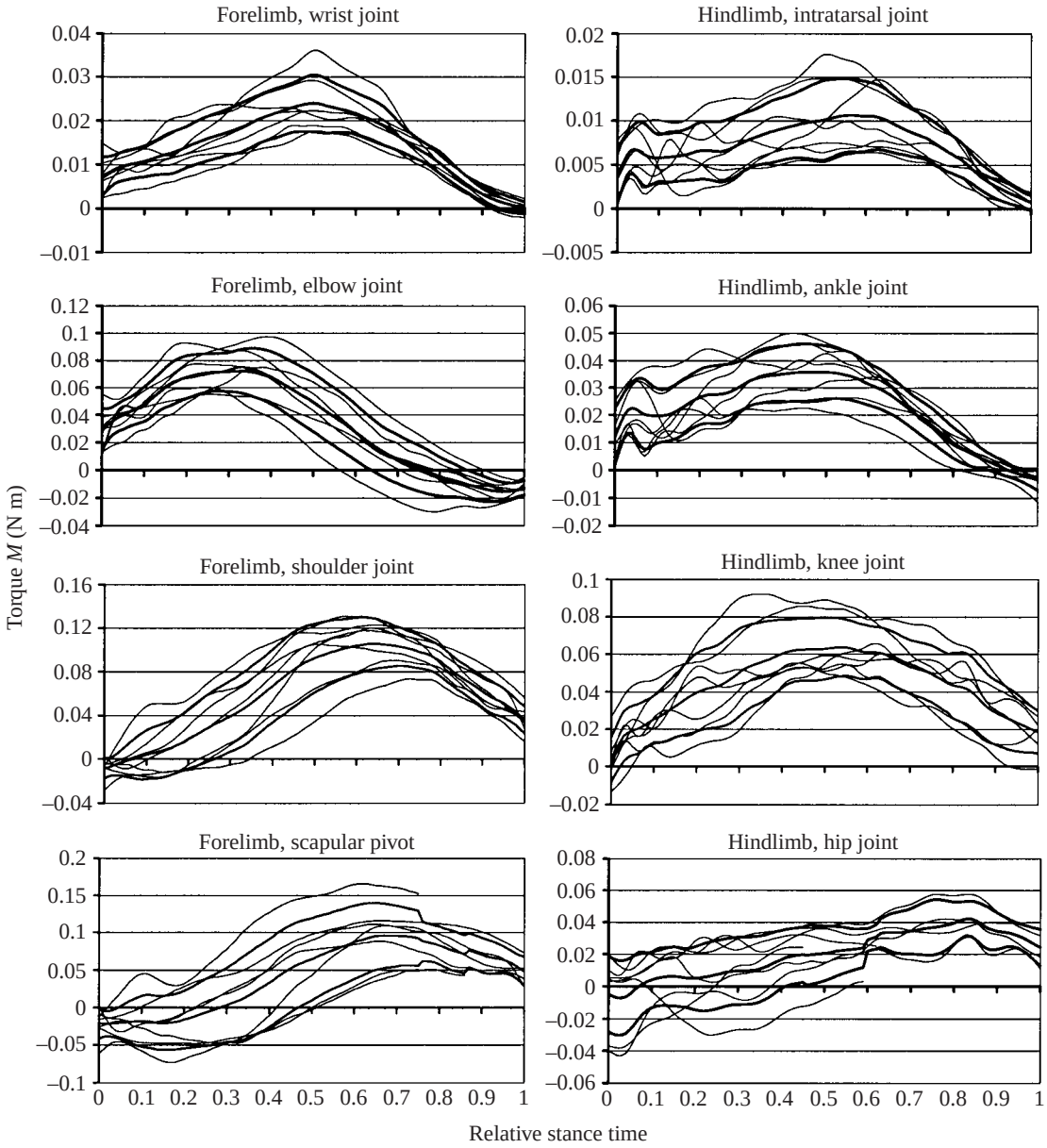


Fig. 6. Torques acting in the main joints of the extremities of a sample of cuis (*Galea musteloides*) during cyclic locomotion. Left, forelimbs; right, hindlimbs. According to a Kolmogorov–Smirnov test, the torques for each relative stance time may be assumed to be normally distributed ($P<0.01$; $N=7$).

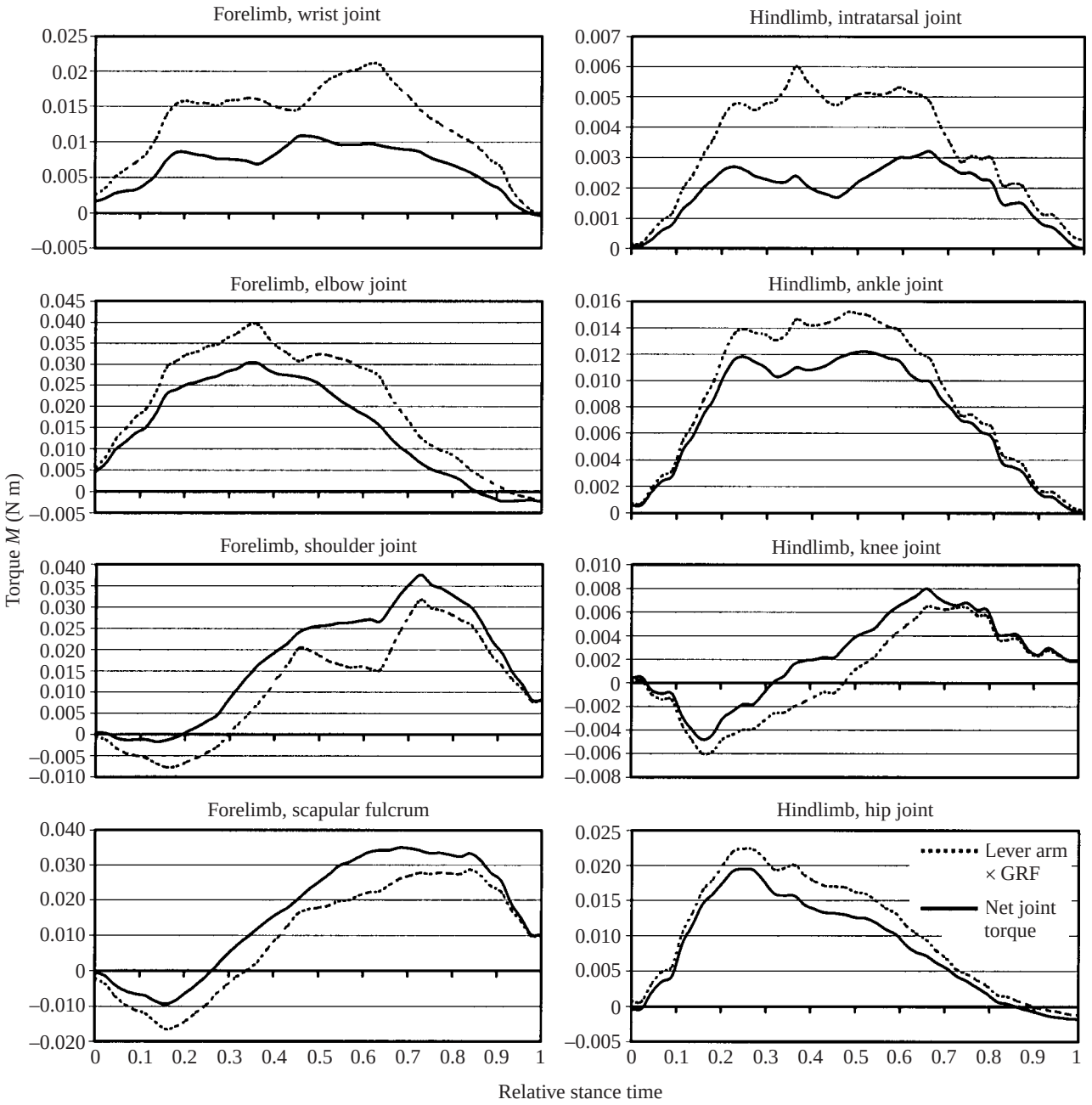


Fig. 7. Proportion of the torques caused by ground reaction forces (GRF) in relation to net joint torques in a half-bounding pika (*Ochotona rufescens*).

(e.g. McMahon, 1985, p. 263: '*Quadrupeds generally use the trot or its variations at moderate speeds, and first the canter and then the gallop as speed increases.*'), these animals and their locomotion are not simply miniaturised versions of large mammals. While medium-sized and large animals change their speed by a factor of 2.6 within a distinct gait, increasing the stride frequency by a factor of 1.6 (cf. Heglund and Taylor, 1988), a typical small animal (*O. rufescens*, the pika) covers a tenfold range of speed (0.13–1.4 m $s^{-1}$) and a fivefold range of frequency (2–10 Hz) within the half-bound (Fischer and Lehmann, 1998).

Our data provide a sound basis for interspecific comparison, despite there being several possible sources for errors. The convergence of data of different species would indicate these errors to be mainly systematic, the identification of which we tried to facilitate by our detailed description of the setup and the quantification of parameters and noise. Additionally, owing to the lower relative masses of the small mammals' distal extremities, the effect of wobbling masses on the joint forces (Gruber et al., 1998), ignored by prevailing standard IDA methods, might predictably be lower in small mammals compared with large mammals.

Fowler et al. (1993) and McCaw and Devita (1995) found that incorrect positioning of GRF on the limb (equivalent to

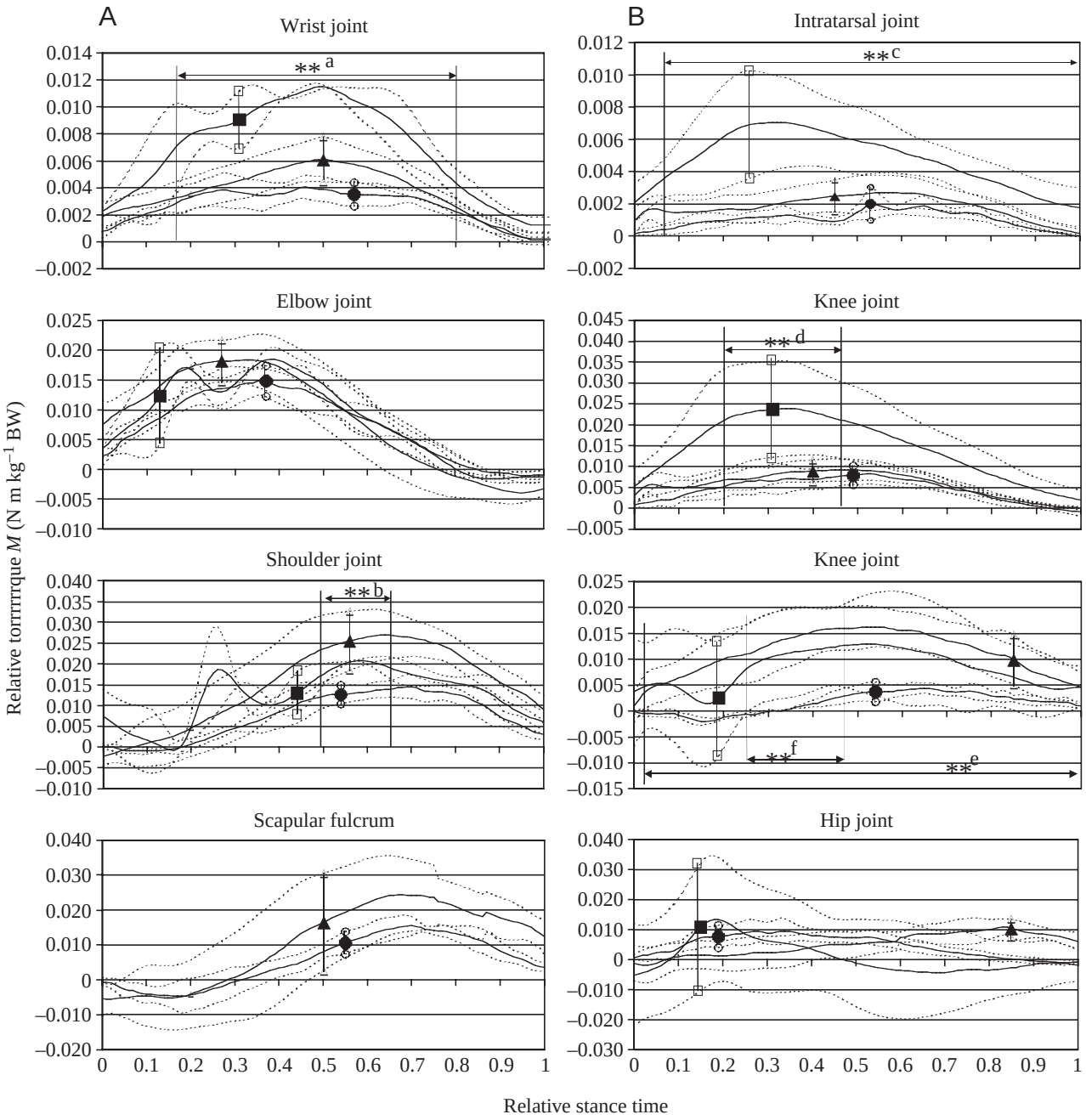


Fig. 8. Torque patterns in the main joints of the extremities of cuis (*Galea musteloides*; triangles, *N*=7), pikas (*Ochotona rufescens*; circles, *N*=3 for forelimb, 4 for hindlimb) and tree shrews (*Tupaia glis*; squares, *N*=2 for forelimb, 5 for hindlimb) during cyclic locomotion. Torques are normalised with reference to body weight (BW). (A) Forelimb, (B) hindlimb. Significant differences ($P$<0.01, Student's $t$ test) are noted by asterisks and letters a–f.

the centre of pressure CoP, if only one single limb is in contact the GRF measuring device) has the largest influence on the accuracy of inverse dynamics calculations. This is due to the fact that the torques produced by GRF are significantly higher than those caused by inertia. Inaccurate positioning of the CoP directly affects the lever arm, one of the two factors determining the torques resulting from GRF.

In contrast, in larger mammals with their extended legs, the application of GRF to an inaccurate CoP underneath hand or foot has a relatively small effect in small mammals, because of their crouched posture and zigzag limb geometry. During midstance, all three proximal elements have a remarkably large lever arm against the dominating vertical GRF, and during lift-off, at least one proximal element is oriented horizontally (e.g. the upper arm) (Fig. 2). The errors remain considerable, but their impact on the errors of IDA is smaller than in larger animals. For the intra- and interindividual variations in cats, Fowler et al. (1993, p. 482) reported that '*a wide variation in*

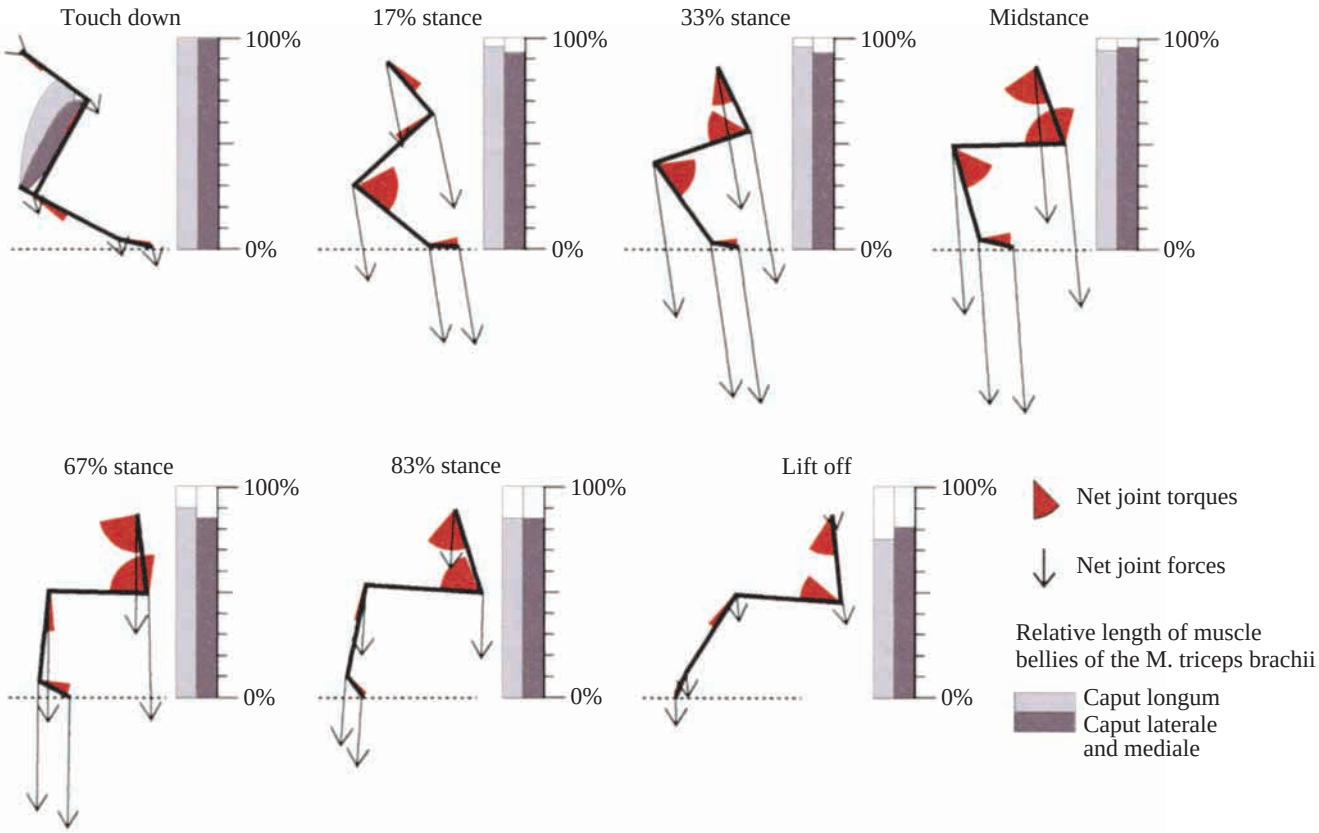


Fig. 9. Dynamics of forelimb motion in the cui (*Galea musteloides*). For seven evenly distributed events during the stance phase, the figure illustrates: the (reactive) net joint forces as vectors; the net joint torques as circle segments, virtually attached to the segment distal of the joint and indicating the rotational tendency by its orientation relative to the segment; and the length of the muscle bellies of M. triceps brachii relative to their length at touch down.

*peak ankle GMMs*' (generalised muscle moments) occurred, while '*the shapes of ankle GMMs were generally similar*.' .

The force effects and the calculated torques conform with the predictions for a quasistatic GRF acting on a four-bar-four-link gear, modelled on kinematic data from our previous studies. What really was surprising was the conformity of time courses of most of the net joint torques in three distantly related mammalian species. This indicates a 'functional convergence' in dynamics every bit as strong as the one identified for kinematics.

Which are the main principles of small mammals' limb dynamics? In the forelimb, all three species conform to the concept of a pantograph leg with central drive and distal tuning mechanism (Fischer and Witte, 1998). The wrist joint lets the forefoot interact with the ground like a bar with a compliant clamped support, its torque graph showing the typical half-sine shape of the rather undamped elongation and consecutive relaxation of a stiff torque spring. Elbow and shoulder joint provide comparable half sine cycles of shorter duration for two-thirds of stance, the maxima occurring when the skeletal element distal of the joint is maximally loaded by body weight. In these three distal joints, the torque has a tendency to extend the joint during the complete or almost complete stance phase, mainly acting against gravity (Fig. 9). This observation is in agreement with the fact that both the mono- and biarticular bellies of the triceps brachii muscle work isometrically, until the lower arm passes the vertical. EMG data (Biedermann et al., 2000; Fischer, 1999; Scholle et al., 1999, 2000) indicate that the lengthening of these muscle bellies after midstance (Fig. 9) is mainly passive, driven by gravity. In the scapular pivot, the flexing torque in early stance indicates a coordinated interaction with the movement of the trunk. The flexing torque in the elbow joint, which might occur at the late stance phase, is again counteracting gravity, which tends to extend the joint after the ground contact has passed the level of the elbow. The protraction of the arm relative to the scapula effectively allows the foot to gain the velocity of the ground, while the caudal part of the animal is lifted causing the airborne phase of the hindlimbs to lengthen. In the late two-thirds of stance, the whole forelimb is retroflected relative to the trunk, with the added effect of a downward sway of the caudal part of the animal. This accelerates the forward swing of the hindlimbs and the occurrence of their ground contact. Thus additionally loaded, the ground contact of a hind limb often shows initial spikes.

The torque patterns on the hindlimbs reveal an important difference between tailed and tail-less species. In the tailed species *T. glis* (preferring synchronous gaits), the hip joint

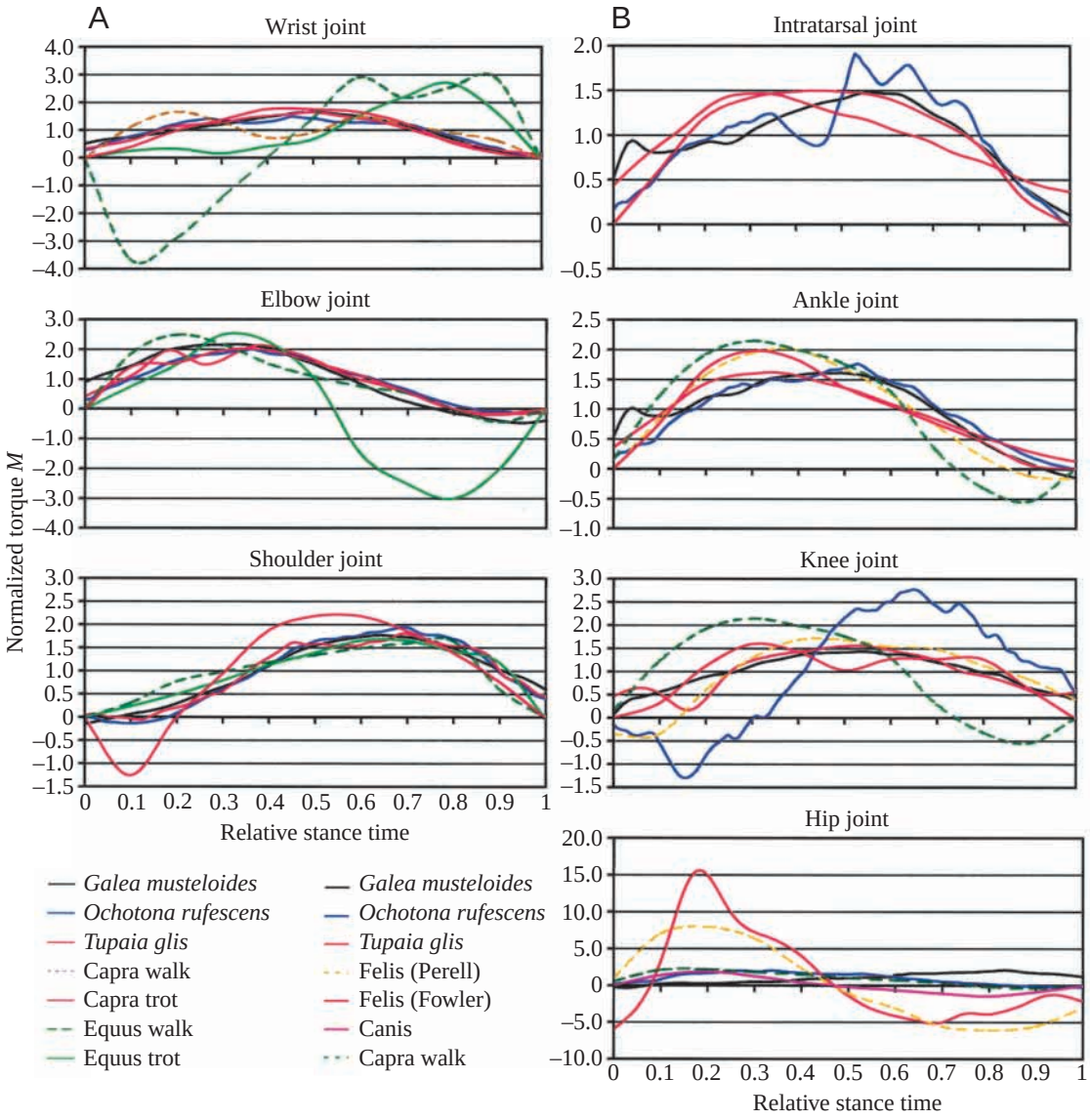


Fig. 10. Torque patterns in the main joints of the extremities of cat (Perell et al., 1988; Fowler et al., 1993), dog (Dogan et al., 1991), goat (Pandy et al., 1988) and horse (Colborne et al., 1997; Clayton et al., 1998) in comparison with the torque patterns of small mammals. (A) Forelimb, (B) hindlimb. Torques are normalised (to 1.0) to a comparable integral of the graph.

mirrors the forelimb in the scapula pivot: the hindlimb perhaps interacts with the tail like the forelimb does with the trunk. Due to the lower mass and mass moment of inertia of the tail compared to the trunk, higher flexing torques are necessary to provoke comparable kinematic effects. The more or less half-sine shape of the knee joint's torque, only in *T. glis*, is overlaid by a higher frequent swinging effect in early stance. The maxima of the torque patterns in the ankle and the intratarsal joint are shifted to early stance, to keep the foot in ground contact by pushing it downward.

The interaction of the tail-less species with the trunk seems to be different. *O. rufescens* (also preferring in-phase gaits) shows a flexion-extension pattern in the knee joint like all the other animals in this study possess in the scapular pivot. The torque in the more proximal hip joint is monophasic with a maximum in late stance, which like that of the knee joint resembles by the torque in the intratarsal joint. The interconnecting ankle joint shows the half-sine pattern of a torque spring. In the other tail-less species, *G. musteloides* (preferring symmetrical gaits without intense kinematic use of the pelvis), all torque patterns are monophasic, the maxima occurring the later the more distal the joint is situated. The two tail-less species have different dynamic hindlimb torque patterns: *O. rufescens* displaces the graded interaction of hindlimb and trunk into the knee joint, while *G. musteloides* pushes the trunk by imposing stronger torques on the segments the more the segments are oriented vertically during the stance phase.

Some of the patterns described can also be found in larger animals: Fig. 10 compares the joint torques acting in the limbs of small mammals with the results of IDA on larger animals available from literature (cat: Perell et al., 1993; Fowler et al., 1993; dog: Dogan et al., 1991; goat: Pandy et al., 1988; horse: Colborne et al., 1997; Clayton et al., 1998). In the distal joints of the hindlimb, cat and goat show torque patterns comparable to those of the small mammals. In the knee joint, the earlier the maximum extending torque occurs in the stance, the larger the animal (and the more extended its hindlimb configuration). The goat, as a large animal,

shows flecting torques in late stance. While the torques in the hip joints of cat (and of dog but to a much lesser extent) are comparable with those observed in the tailed small mammal *T. glis*, the hip joint of the goat acts more in the fashion of that of the tail-less pika. Hence, the presence or absence of a tail affects dynamics in a way that is independent of body size.

In the forelimb, the situation is more complicated. Data for the scapula are completely absent in other studies, because it has simply been overlooked as the main propulsive pivot. In the shoulder joint walking and running goats show a torque pattern comparable with that of small mammals. The trotting horse shows a short initial burst of flexion, the consecutive maximal extending torques occur in midstance, earlier than in the other animals. In the fetlock joint (analogous to the wrist joint) and in the elbow joint, the trotting horse exhibits torque patterns that are quite similiar to those of small mammals. In the walking horse this pattern in the fetlock joint is superimposed by the typical M-shape of the ground reaction force graph (well-known from human walking). But, in contrast to this similarity of torques in the distal joints of the forelimb in small and large mammals, for the medium-sized goat, the maxima of extending torques in the distal joints are reported to occur in late stance. In the elbow joint of the trotting goat during the second half of the stance a flexing torque was determined. In our opinion this result is not compatible with the needs of antigravitational actions to prevent the leg from collapsing. Further work has to be undertaken to understand the locomotion of the medium-sized goat.

The dynamic patterns of small mammals are coupled to the use of the rectangular, zigzag-shaped 'pantograph' leg construction with more or less 1:1 relationship of the segments' lengths (Fischer and Witte, 1998; for a basic explanation of the ratio, cf. Witte et al., 1991; Seyfarth et al., 2001). The limitations of an upscaling of this construction for larger animals are attributed to the growing gap between loads (G prop. m) and muscular capabilities (F prop. $m^{2/3}$) for these animals, forcing them to extend their legs in order to shorten the lever arms for a muscular withstanding of external loads (cf. Biewener, 1989). However, recent hyraxes illustrate well the constraint onto a zigzag limb geometry in small mammals. They are most probably descendants of Miocene cursorial forms, which are thought to have been at least the size of a large goat (Fischer, 1992). After secondarily becoming smaller, they now have the 'usual' zigzag-shaped limbs of small therian mammals.

Professor Dr H.-R. Duncker (University of Gießen) and Dr Alain Puget (University of Toulouse) made living animals for functional analyses accessible to us. Dr L. Peichel (Max-Planck-Institut für Hirnforschung, Frankfurt/Main) provided a dead animal for morphometrics. Dr Haarhaus (IWF Göttingen) made the cineradiographies possible. Professors Dr W. Thonfeld and Dipl.-Ing. K. Urban (Fachhochschule Jena) carried out the laser-scanning volumetry of the animals' segments, Priv.-Doz. Dr M. Jergas (Ruhr-Universität Bochum) provided opportunities for us to carry out CT and MRI scanning. We thank all those colleagues for unreserved cooperation. We are grateful to M. Roser for creating the figure on the stance-phase characteristics of the cui's forelimb. The study was funded by the Deutsche Forschungsgemeinschaft (DFG) (Innovationskolleg 'Bewegungssysteme' Teilprojekt B1) and Schwerpunktprogramm ('Autonomes Laufen' Fi 410/4-1).

## References

**Alexander, R. M.** (1988). *Elastic Mechanisms in Animal Locomotion*. Cambridge: Cambridge University Press.

**Alexander, R. M. and Goldspink, G.** (1977). *Mechanics and Energetics of Animal Locomotion*. London: Chapman and Hall.

**Andrews, J. G. and Mish, S. P.** (1996). Methods for investigating the sensitivity of joint resultants to body segment parameter variations. *J. Biomech.* **29**, 654.

**Bergmann, G., Graichen, F. and Rohlmann, A.** (1993). Hip joint loading during walking and running, measured in two patients. *J. Biomech.* **26**, 969–990.

**Biedermann, F. H. W., Schumann, N. P., Fischer, M. S. and Scholle, H.-C.** (2000). Surface EMG-recordings using a miniaturised matrix electrode: a new technique for small animals. *J. Neurosci Methods* **97**, 69–75.

**Biewener, A. A.** (1989). Scaling body support in mammals: limb posture and muscle mechanics. *Science* **245**, 45–48.

**Biewener, A. A. and Baudinette, R.** (1995). In vivo muscle force and elastic energy storage during steady-speed hopping of tammar wallabies (*Macropus eugenii*). *J. Exp. Biol.* **189**, 1829–1841.

**Biewener, A. A., Blickhan, R., Perry, A. K., Heglund, N. C. and Taylor, C. R.** (1988). Muscle forces during locomotion in kangaroo rats: force platform and tendon buckle measurements compared. *J. Exp. Biol.* **137**, 191–205.

**Brand, R. A., Pedersen, D. R., Davy, D. T., Kotzar, G. M., Heiple, K. G. and Goldberg, V. M.** (1994). Comparison of hip force calculations and measurements in the same patient. *J. Arthroplasty* **9**, 45–51.

**Bresler, B. and Frankel, J. P.** (1950). The forces and moments in the leg during level walking. *Trans. Am. Soc. Mech. Eng.* **72**, 27–36.

**Calder, W. A.** (1984). *Size, Function and Life History*. Mineola: Dover Publications.

**Cavagna, G. A., Heglund, N. C. and Taylor, C. R.** (1977). Mechanical work in terrestrial locomotion: two basic mechanisms for minimizing energy expenditure. *Am. J. Physiol.* **233**, 243–261.

**Challis, J. H.** (1997). Producing physiologically realistic individual muscle force estimations by imposing constraints when using optimization techniques. *Med. Eng. Phys.* **19**, 253–261.

**Chang, Y. H., Huang, H.-W., Hamerski, C. M. and Kram, R.** (2000). The independent effects of gravity and inertia on running mechanics. *J. Exp. Biol.* **203**, 229–238.

**Clayton, H. M., Lanovaz, J. L., Schamhardt, H. C., Willemen, M. A. and Colborne, G. R.** (1998). Net joint moments and powers in the equine forelimb during the stance phase of the tort. *Equine Vet. J.* **30**, 384–389.

**Colborne, G. R., Lanovaz, J. L., Sprigings, E. J., Schamhardt, H. C. and Clayton, H. M.** (1997). Joint moments and power in equine gait: a preliminary study. *Equine Vet. J.* **23 (Suppl.)**, 33–36.

**Dogan, S., Manley, P. A., Vanderby, R., Kohles, S. S., Hartman, L. M. and McBeath, A. A.** (1991). Canine intersegmental hip joint forces and moments before and after cemented taotal hip replacement. *J. Biomech.* **24**, 397–407.

**Eng, J. J. and Winter, D. A.** (1995). Kinetic analysis of the lower limbs during walking: what information can be gained from a three-dimensional model? *J. Biomech.* **28**, 753–758.

**Fischer, M. S.** (1992). Hyracoidea. In *Handbuch derZoologie. Band VIII (Mammalia)* (ed. D. Starck, H. Schliemann and J. Niethammer). *Teilband* **58**, 1–169.

**Fischer, M. S.** (1994). Crouched posture and high fulcrum. A principle in the locomotion of small mammals: the example of the rock hyrax (*Procavia capensis*) (Mammalia: Hyracoidea). *J. Human Evol.* **26**, 501–524.

**Fischer, M. S.** (1998). Die Lokomotion von *Procavia capensis* (Mammalia: Hyracoidea). Ein Beitrag zur Evolution des Bewegungssystems der Säugetiere. *Abh. Naturwiss. Verh. naturwiss. Vereins Hamburg (NF)* **33**, 1–188.

**Fischer, M. S.** (1999). Kinematics, EMG, and inverse dynamics of the Therian forelimb – a synthetic approach. *Zool. Anz.* **238**, 41–54.

**Fischer, M. S. and Lehmann, R.** (1998). Application of cineradiography for the metric and kinematic study of in-phase gaits during locomotion of the pika (*Ochotona rufescens*, Mammalia: Lagomorpha). *Zoology* **101**, 12–37.

**Fischer, M. S., Schilling, N., Schmidt, M., Haarhaus, D. and Witte, H.** (2002). Basics limbs kinematics of small therian mammals. *J. Exp. Biol.* **205**, 1315–1338.

**Fischer, M. S. and Witte, H.** (1998). The functional morphology of the three-segmented limb of mammals and its specialities in small and medium-sized mammals. *Proc. Eur. Mech. Coll. Euromech. (Biology and Technology of Walking)* **375**, 10–17.

**Fowler, E. G., Gregor, R. J., Hodgson, J. A. and Roy, R. R.** (1993). Relationship between ankle muscle and joint kinetics during the stance phase of locomotion in the cat. *J. Biomech.* **26**, 465–483.

**Full, R. J. and Koditschek, D. E.** (1999). Templates and anchors: neuromechanical hypotheses of legged locomotion on land. *J. Exp. Biol.* **202**, 3325–3332.

**Full, R. J., Blickhan, R. and Ting, L. H.** (1991). Leg design in hexapedal runners. *J. Exp. Biol.* **158**, 369–390.

**Fung, Y. C.** (1993). *Biomechanics*. 2nd edition. Berlin: Springer.

**Ganor, I. and Golani, I.** (1980). Coordination and integration in the hindleg step cycle of the rat: kinematic synergies. *Brain Res.* **195**, 57–67.

**Glitsch, U. and Baumann, W.** (1997). The three-dimensional determination of internal loads in the lower extremity. *J. Biomech.* **30**, 1123–1131.

**Graichen, F. and Bergmann, G.** (1988). A telemetric transmission system for in vivo measuring of hip joint force with instrument-implanted prostheses. *Biomed. Tech.* **33**, 305–312.

**Graichen, F. and Bergmann, G.** (1991). Four-channel telemetry system for in vivo measurement of hip joint forces. *J. Biomed. Eng.* **13**, 370–374.

**Gregor, R. J. and Abelew, T. A.** (1994). Tendon force measurements and movement control: a review. *Med. Sci. Sports Exerc.* **26**, 1359–1372.

**Gruber, K., Ruder, H., Denoth, J. and Schneider, K.** (1998). A comparative study of impact dynamics: wobbling mass model versus rigid body models. *J. Biomech.* **31**, 439–444.

**Hatze, H.** (1981). The use of optimally regularized Fourier series for estimating higher order derivatives of noisy biomechanical data. *J. Biomech.* **14**, 13–18.

**Heglund, N. C., Taylor, C. R. and McMahon, T. A.** (1974). Scaling stride frequency and gait to animal size: mice to horses. *Science* **186**, 1112–1113.

**Heglund, N. C., Cavagna, G. A. and Taylor, C. R.** (1982). Energetics and mechanics of terrestrial locomotion. III. Energy changes of the center of mass as a function of speed and body size in birds and mammals. *J. Exp. Biol.* **79**, 41–56.

**Heglund, N. C. and Taylor, C. R.** (1988). Speed, stride frequency and energetic cost per stride: how do they change with body size and gait? *J. Exp. Biol.* **138**, 301–318.

**Hoy, M. G. and Zernicke, R. F.** (1985). Modulation of limb dynamics in the swing phase of locomotion. *J. Biomech.* **18**, 49–60.

**Jansen, M. O., van den Bogert, A. J., Riemersma, D. J. and Schamhardt, H. C.** (1993). In vivo tendon forces in the forelimb of ponies at the walk, validated by ground reaction force measurements. *Acta Anat.* **146**, 162–167.

**Koopman, B., Grootenboer, H. J. and De Jongh, H. J.** (1995). An inverse dynamics model for the analysis, reconstruction and prediction of bipedal walking. *J. Biomech.* **28**, 1369–1376.

**Kotzar, G. M., Davy, D. T., Goldberg, V. M., Heiple, K. G., Berilla, J., Heiple, K. G. Jr., Brown, R. H. and Burstein, A. H.** (1991). Telemeterized in vivo hip joint force data: a report on two patients after total hip surgery. *J. Orth. Res.* **9**, 621–633.

**Krabbe, B., Farkas, R. and Baumann, W.** (1997). Influence of inertia on intersegment moments of the lower extremity joints. *J. Biomech.* **30**, 517–519.

**Kuznetzov, A. N.** (1995). Energetical profit of the third segment in parasagittal legs. *J. Theor. Biol.* **172**, 95–105.

**Malaviya, P., Butler, D. L., Korvick, D. L. and Proch, F. S.** (1998). In vivo tendon forces correlate with activity level and remain bounded: evidence in a rabbit flexor tendon model. *J. Biomech.* **31**, 1043-1049.

**Manter, J. T.** (1938). The dynamics of quadrupedal walking. *J. Exp. Biol.* **15**, 522–540.

**McCaw, S. T. and Devita, P.** (1995). Errors in alignment of center of pressure and foot coordinates affect predicted lower extremity torques. *J. Biomech.* **28**, 985–988.

**McMahon, T. A.** (1985). The role of compliance in mammalian running gaits. *J. Exp. Biol.* **115**, 263–282.

**Nagano, A., Gerritsen, K. G. M. and Fukashiro, S.** (2000). A sensitivity analysis of the calculation of mechanical output through inverse dynamics: a computer simulation study. *J. Biomech.* **33**, 1313-1318.

**Pandy, M. G., Kumar, V., Berme, N. and Waldron, K. J.** (1988). The dynamics of quadrupedal locomotion. *J. Biomech. Eng.* **110**, 230–237.

**Pedley, T. J.** (1977). *Scale Effects in Locomotion*. London: Academic Press.

**Perell, K. L., Gregor, R. J., Buford, J. A. and Smith, J. L.** (1993). Adaptive control for backward quadrupedal walking. IV. Hindlimb kinetics during stance and swing. *J. Neurophysiol.* **70**, 2226–2240.

**Plagenhoeft, S.** (1979). Biomechanical analysis of Olympic flatwater kayaking and canoeing. *Res. Q.* **50**, 443–459.

**Schilling, N. and Fischer, M. S.** (1999). Kinematic analysis of treadmill locomotion of tree shrews, *Tupaia glis* (Scandentia: Tupaiidae). *Z. Saeugetierk.* **64**, 129–153.

**Schmidt, M. and Fischer, M. S.** (2000). Cineradiographic study of forelimb movements during quadrupedal walking in the Brown Lemur (*Euleumur fulvus*, Primates: Lemuridae). *Am. J. Phys. Anthropol.* **111**, 245–262.

**Scholle, H.-C., Biedermann, F. H. W., Schumann, N. P., Roeleveld, K., Stegeman, D. F., Schilling, N. and Fischer, M. S.** (1999). Morphofunctional relations in triceps brachii muscle of small mammals during treadmill locomotion. *Pflügers Arch. Eur. J. Physiol.* **437**, R127.

**Scholle, H.-C., Schumann, N. P., Biedermann, F. H. W., Grassme, R., Roeleveld, K., Stegeman, D. F., Schilling, N. and Fischer, M. S.** (2000). The selective activation of rat triceps brachii muscle during defined locomotion – relation to the three-dimensional muscle fibre distribution. *Pflügers Arch. Eur. J. Physiol.* **439**, R291.

**Seyfarth, A., Gunther, M. and Blickhan, R.** (2001). Stable operation of an elastic three-segment leg. *Biol. Cybern.* **84**, 365-382.

**Taylor, C. R., Heglund, N. C. and Maloiy, G. M. O.** (1982). Energetics and mechanics of terrestrial locomotion. I. Metabolic energy consumption as a function of speed and body size in birds and mammals. *J. Exp. Biol.* **92**, 1–21.

**Winter, D. A.** (1990). *Biomechanics and Motor Control of Human Movement*. New York: John Wiley and Sons.

**Witte, H., Ostendorf, U. and Bellenberg, B.** (1997). Muskelkraftmessung mittels Kernspin-Spektroskopie. *Biomed. Tech. (Berlin)* **42 (Suppl. 2)**, 79–80.

**Witte, H., Preuschoft, H. and Recknagel, S.** (1991). Biomechanical factors that influence the overall human body shape. *Z. Morph. Anthrop.* **78**, 407-423.